Development of a protein signature to enable clinical positioning of IAP inhibitors in colorectal cancer

McCann, C., Matveeva, A., McAllister, K., Van Schaeybroeck, S., Sessler, T., Fichtner, M., Carberry, S., Rehm, M., Prehn, J. H. M., & Longley, D. B. (2021). Development of a protein signature to enable clinical positioning of IAP inhibitors in colorectal cancer. *The FEBS Journal*, *288*(18), 5374-5388. https://doi.org/10.1111/febs.15801

Document Version:
Publisher's PDF, also known as Version of record

Queen's University Belfast - Research Portal:
Link to publication record in Queen's University Belfast Research Portal

Development of a protein signature to enable clinical positioning of IAP inhibitors in colorectal cancer

Christopher McCann[1] (iD), Anna Matveeva[2] (iD), Katherine McAllister[1], Sandra Van Schaeybroeck[1], Tamas Sessler[1], Michael Fichtner[2] (iD), Steven Carberry[2], Markus Rehm[3] (iD), Jochen H.M. Prehn[2] and Daniel B. Longley[1] (iD)

1 Patrick G. Johnston Centre for Cancer Research, Queen's University Belfast, UK
2 Department of Physiology & Medical Physics and Centre for Systems Medicine, Royal College of Surgeons in Ireland (RCSI) University of Medicine and Health Sciences, Dublin, Ireland
3 Institute of Cell Biology and Immunology, University of Stuttgart, Germany

Resistance to chemotherapy-induced cell death is a major barrier to effective treatment of solid tumours such as colorectal cancer, CRC. Herein, we present a study aimed at developing a proteomics-based predictor of response to standard-of-care (SoC) chemotherapy in combination with antagonists of IAPs (inhibitors of apoptosis proteins), which have been implicated as mediators of drug resistance in CRC. We quantified the absolute expression of 19 key apoptotic proteins at baseline in a panel of 12 CRC cell lines representative of the genetic diversity seen in this disease to identify which proteins promote resistance or sensitivity to a model IAP antagonist [birinapant (Bir)] alone and in combination with SoC chemotherapy (5FU plus oxaliplatin). Quantitative western blotting demonstrated heterogeneous expression of IAP interactome proteins across the CRC cell line panel, and cell death analyses revealed a widely varied response to Bir/chemotherapy combinations. Baseline protein expression of cIAP1, caspase-8 and RIPK1 expression robustly correlated with response to Bir/chemotherapy combinations. Classifying cell lines into 'responsive', 'intermediate' and 'resistant' groups and using linear discriminant analysis (LDA) enabled the identification of a 12-protein signature that separated responders to Bir/chemotherapy combinations in the CRC cell line panel with 100% accuracy. Moreover, the LDA model was able to predict response accurately when cells were cocultured with Tumour necrosis factor-alpha to mimic a pro-inflammatory tumour microenvironment. Thus, our study provides the starting point for a proteomics-based companion diagnostic that predicts response to IAP antagonist/SoC chemotherapy combinations in CRC.

Abbreviations

5FU, 5-Fluorouracil; APAF-1, Apoptosis-associated factor-1; Bak, BCL2 antagonist/killer; Bax, BCL2-associated X-protein; Bcl-2, B-cell lymphoma 2; Bir, Birinapant; CRC, Colorectal cancer; FADD, Fas-associated death domain; FLIP, FADD-like IL-1β-converting enzyme inhibitory protein; IAP, Inhibitor of apoptosis; LDA, Linear discriminatory analysis; MCL-1, Myeloid cell leukaemia differentiation protein 1; MLKL, Mixed lineage kinase domain-like pseudokinase; MOMP, Mitochondrial outer membrane permeabilisation; PCA, Principal component analysis; RIPK1/3, Receptor-interacting protein kinase 1/3; SMAC, Second mitochondria-derived activator of caspases; SoC, Standard of care; TNF-α, Tumour necrosis factor-alpha; XIAP, X-Linked inhibitor of apoptosis protein.

Introduction

Resistance to apoptosis is a classical hallmark of cancer, which can manifest clinically as lack of response to chemotherapeutic agents such as 5-Fluorouracil (5FU) and oxaliplatin [1]. Cancer cells can acquire such resistance through increasing their expression of (and therefore dependence on) anti-apoptotic proteins such as inhibitor of apoptosis proteins (IAPs), making such proteins attractive therapeutic targets [2]. IAPs exert their anti-apoptotic function via two distinct mechanisms [3]. Firstly, cIAP1 and cIAP2 can divert typically death-inducing Tumour necrosis factor-alpha (TNF-α) signals to prosurvival signalling through the ubiquitination of RIPK1, leading to the activation of Nuclear factor kappa-B transcriptional programmes that enhance cell proliferation, propagate further inflammatory signalling via transcriptional upregulation of cytokines including TNF-α itself and drive the transcription of anti-apoptotic proteins, including the caspase-8 regulator FADD-like IL-1β-converting enzyme inhibitory protein (FLIP) and the IAPs themselves [4,5]. Secondly, IAPs [specifically X-Linked inhibitor of apoptosis protein (XIAP)] can directly inhibit the complete processing and subsequent activation of caspase-3/7 and caspase-9, thereby abrogating the cell's ability to execute apoptosis [6,7].

IAP antagonists interact with IAPs through binding to their BIR domains and promote apoptosis induced by extracellular death ligands such as TNF-α by inhibiting cIAP-induced RIPK1 ubiquitination [3,8]; this leads to the formation of an intracellular death signalling complex termed complex II in which RIPK1 recruits Fas-associated death domain (FADD), which in turn recruits procaspase-8 and FLIP. Depending on the relative amounts of procaspase-8 and FLIP in this complex, procaspase-8 can form homodimers, which drive apoptosis [9,10]. In the absence of procaspase-8, this complex can instead activate necroptosis [11], an alternative form of programmed cell death in which RIPK1 recruits and activates RIPK3 eventually leading to phosphorylation of Mixed lineage kinase domain-like pseudokinase (MLKL); phosphorylated MLKL oligomerises and forms pores in the plasma membrane that result in pro-inflammatory cell lysis [12]. IAP antagonists also inhibit XIAP facilitating apoptosis mediated by the intrinsic mitochondrial apoptotic pathway and the execution phase of apoptosis mediated by caspase-3/7 [13,14].

The clinical realisation of the potential of IAP antagonists has been hampered by the lack of predictive biomarkers of response to enable patient stratification. Using a large panel of colorectal cancer (CRC)

cell lines representative of the clinical diversity seen in CRC, herein we have developed a strategy to predict responses to IAP antagonist-based therapy by quantifying the expression of key apoptotic proteins.

Results and Discussion

Response of CRC cell lines to IAP antagonist-based therapy

We assembled a panel of 12 CRC cell lines with a range of genotypes and microsatellite status (Table 1) that were co-treated with a model IAP antagonist birinapant (Bir, TL37211) alone and in combination with 5FU and oxaliplatin ('OX5FU', to mimic the clinical FOLFOX regimen). In addition, we included treatment arms in which a pro-inflammatory tumour microenvironment was modelled using recombinant TNF-α. Cell death was quantified after treatment for 24, 48 or 72 h; the average cell death was also calculated over the three time points (Fig. 1).

Overall, the cell lines were resistant to Bir alone, with GP5D demonstrating the greatest apoptotic response of just 25% averaged across the three time points (Fig. 1). Although TNF-α alone induced nonsignificant levels of cell death, its addition to Bir significantly increased apoptosis; again, GP5D cells were most sensitive to Bir/TNF-α with ~60% apoptosis at 24 h and ~80% at 48 h. A range of responses were observed in the models, with only the COLO320 model completely resistant to Bir/TNF-α at all time points.

Compared to Bir/TNF-α, OX5FU-induced apoptosis had slower kinetics, with the greatest degree of

Table 1. Genotype of panel of 12 colon cancer cell lines.

Mutations	TP53	RAS	BRAF	PIK3CA	MSI
DLD1	S241F	G13D	WT	E545K; D549N	Y
LS174T	WT	G12D	WT	H1047R	Y
LoVo	WT	G13D; A14V	WT	WT	Y
HT29	R273H	WT	V600E	P449T	N
GP5D	WT	WT	WT	E545K	Y
LIM1215	WT	WT	WT	WY	Y
HCT116	WT	G13D	WT	H1047R	Y
RKO	WT	WT	V600E	WT	Y
SW620	R273H; P309S	G12V	WT	WT	N
COLO320	R248W	WT	WT	WT	Y
LS513	WT	G12D	WT	WT	N
HCT116 p53−/−	NULL	G13D	WT	H1047R	Y
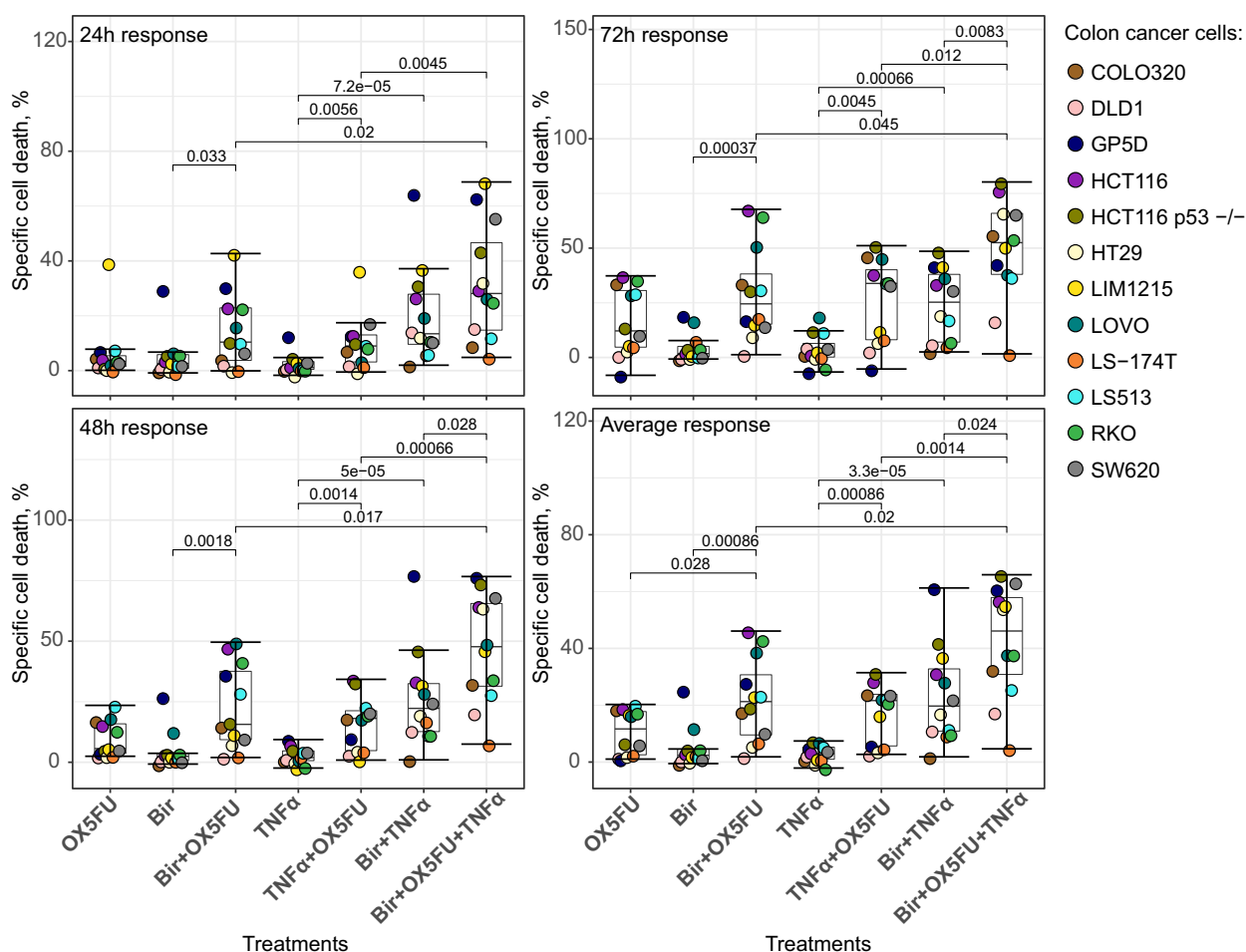
Fig. 1. Specific cell death in 12 colon cancer cell lines upon seven combinational treatments. 24, 48 and 72 h and averaged over three time points of specific cell death are shown for TNF-α, OX5FU and Bir combinational treatments. Individual cell lines depicted by coloured dots. Boxplot represents interquartile range (IQR) with the median, 25% (Q1) and 75% (Q3) quantiles as middle, lower and upper hinges, respectively. Lower and upper whiskers are Q1-1.5*IQR and Q3+1.5*IQR, respectively. *P*-values of the mean response comparison by the Wilcoxon test without correction are indicated for significantly different treatment responses.

cell death observed at 72 h; however, over half of the models exhibited a high level of resistance to this treatment (which mimics the clinical standard-of-care regimen), with < 10% cell death even at 72 h. It was notable therefore that the apoptotic response to chemotherapy of a number of models was significantly enhanced by the co-treatment with Bir, including LoVo, RKO and HCT116 (Fig. 1). In the context of TNF-α, there were further increases in cell death observed in cells co-treated with Bir and OX5FU in several models, including SW620, p53 null HCT116, HT29 and LIM1215.

Fig. 2. Protein quantification. (A) Schematic representation of apoptosis signalling pathway depicting the sequence of interactions between all apoptotic proteins quantified. (B), (i) Western blot images and associated densitometry standard curve for concentration ranges of recombinant IAP interactome proteins (p-18 subunit caspase-8, FADD, RIPK1, RIPK3, FLIP, XIAP, cIAP1, cIAP2) alongside increasing range of HeLa (or HT29) reference lysate from which absolute protein concentrations could be interpolated onto standard curve based on densitometries, (ii & iii) summary of absolute concentrations of proteins in HeLa or HT29 cell lysate. (C) Representative western blot panels for cIAP1, cIAP2, XIAP, RIPK1, RIPK3*, FADD, procaspase-8, FLIP(L), FLIP(S), BID, BCL-2, BCL-XL, MCL-1, BAK, BAX, APAF1, procaspase-9, SMAC and procaspase-3 in 30 µg CRC cell line lysate alongside increasing amounts of HeLa reference lysate for quantification. Protein font colour corresponds with that in Fig. 2A. *RIPK3 is absent from HeLa; therefore, CRC cell line absolute RIPK3 abundance was calculated using HT29 as a reference. Western blot images and densitometry are representative of three independent experiments, and quantification represents the mean ± SEM of three independent experiments.

Table 2. Protein concentration profile for 12 colon cancer cell lines. Concentrations determined by quantitative western blotting in μM scale.

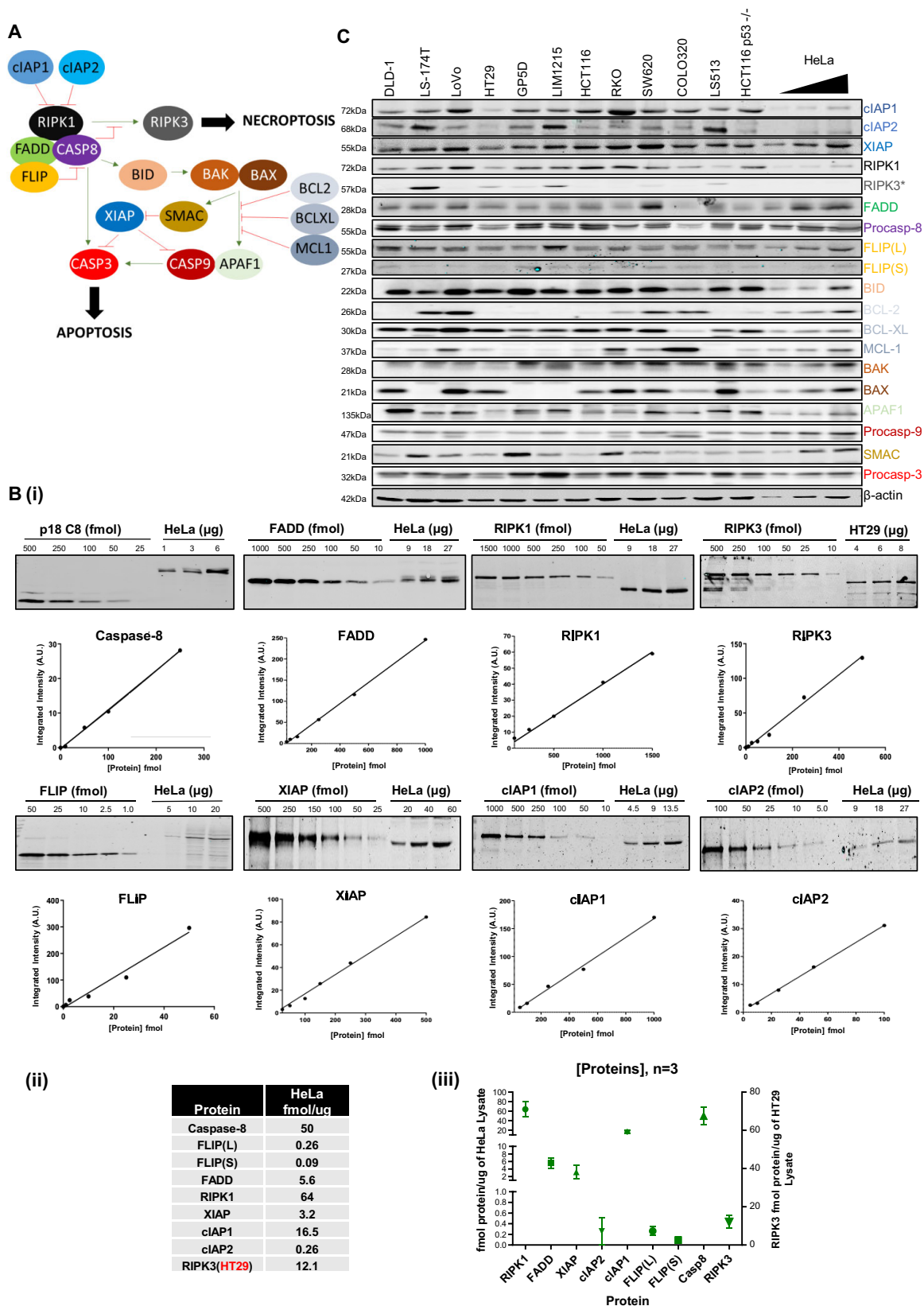| DLD1	LS174T	LOVO	HT29	GP5D	LIM1215	HCT116	RKO	SW620	COLO320	LS513	HCT p53−/−	
4.6	2.8	10	1.2	8.9	8.4	14.1	19.4	4.54	11.5	3	11.7	cIAP1
0.19	0.32	0.11	0.01	0.22	0.82	0.13	0.1	0.15	0.17	0.36	0.09	cIAP2
0.13	0.1	0.2	0.1	0.13	0.25	0.25	0.26	0.42	0.21	0.08	0.12	XIAP
51	37	107	25	92	112	195	94	38	53	9.6	105	RIPK1
0.1	8.31	0.07	0.84	0.37	3.6	0.13	0.02	0.19	0.08	0.47	0	RIPK3
0.27	0.11	0.19	0.14	0.24	0.27	0.44	0.12	0.29	0.11	0.08	0.15	FADD
3.19	1.9	2.89	1.93	4.91	4.38	6.37	1.64	1.5	1.74	1.66	4.48	CASP8
0.04	0.03	0.04	0.03	0.02	0.08	0.03	0.03	0.02	0.04	0.01	0.02	FLIP(L)
0.02	0	0	0.01	0	0	0.06	0	0	0	0.01	0.01	FLIP(S)
1.86	0.67	3.12	1.29	3.79	1.52	1.49	1.46	1.39	0.39	0.65	1.12	BID
0	0.05	0.11	0	0	0	0	0.01	0.05	0.05	0	0.01	BCL-2
0.33	0.27	0.58	0.33	0.17	0.24	0.31	0.32	0.32	0.05	0.12	0.24	BCL-XL
0.03	0.05	0.21	0.06	0.01	0.02	0.03	0.15	0.12	0.74	0.01	0.05	MCL-1
0.98	3.5	2.4	1.24	6.44	2.07	0.66	4.33	1.51	1.26	0.65	0.91	BAK
0.61	0.04	0.91	0.51	0.01	0	0.4	0.6	0.42	0.23	0.76	0.19	BAX
5.8	1.3	2.43	0.89	2.05	2.53	1.48	1.16	1.48	1.65	1.45	2.26	APAF1
0.03	0.03	0.02	0.01	0.02	0.02	0.02	0.01	0.13	0.01	0.02	0.02	CASP9
0.13	0.46	0.32	0.14	1.03	0.32	0.09	0.6	0.2	0.17	0.1	0.12	SMAC
0.07	0.07	0.05	0.05	0.1	0.14	0.08	0.1	0.12	0.14	0.09	0.1	CASP3

Protein font colours correspond to those in apoptosis signalling schematic Fig. 2.

Apoptotic protein expression profiling

In order to better understand the heterogeneity of response to IAP inhibitors in CRC, the absolute expression of a panel of key IAP interactome and other major apoptotic regulators (Fig. 2A) was determined by quantitative western blotting. Absolute protein levels were quantified by initially determining the concentrations of these proteins within a reference cell line (HeLa or HT29) by comparison to recombinant proteins as described previously [16,18]. We generated a concentration range of recombinant proteins against which could be used to calculate the concentration of target proteins in the reference cell line (Fig. 2B). Protein concentrations in each CRC model were then determined by western blotting, with comparison of each protein in each model against the protein levels in the reference cell line (Fig. 2C). This allowed us to obtain absolute concentrations for each protein in each CRC model (Table 2).

Not surprisingly given the heterogeneity of CRC and the heterogeneity of responses to Bir, the levels of key proteins of the extrinsic apoptotic pathway (procaspase-8, FLIP(L), FLIP(S), FADD, RIP1, RIP3, Cellular inhibitor of apoptosis protein 1/2, XIAP) were variable across the panel of cell lines (Fig. 2B, Table 2). cIAP1 was present in all models and expressed at a consistently higher level than cIAP2 and XIAP. RIPK1 was the most highly expressed protein in the panel, whereas RIPK3 was expressed at a much lower level overall and

was absent or almost completely absent in five models. The key adaptor protein for complex II, FADD, was similarly expressed across the cell line panel. Notably, the key apoptotic effector of the extrinsic pathway caspase-8 was expressed at a relatively high level in all models. The long splice form (FLIP(L)) of the canonical regulator of caspase-8, FLIP, was expressed at a relatively low level in comparison with procaspase-8, and the short splice form FLIP(S) was absent in several models; this is consistent with the findings of us and others that FLIP expression can be > 100-fold lower than procaspase-8, although it can still compete effectively with procaspase-8 for recruitment to effector complexes such as the DISC [26].

We also used previously established [16,18] concentrations in HeLa cells for B-cell lymphoma 2 (Bcl-2) family proteins, procaspase-3 and procaspase-9, APAF1 and Second mitochondria-derived activator of caspases (SMAC) to determine the levels of these key regulators of mitochondrial apoptosis in the CRC panel (Fig. 2A,B, Table 2). The Bcl-2 family regulate mitochondrial outer membrane permeabilisation (MOMP), a critical commitment point in apoptosis induction [27]. For the Bcl-2 family of proteins, it was notable that BID, which mediates cross-talk between the extrinsic and intrinsic mitochondrial pathways [28], was expressed at a consistent, relatively high level across the panel. The key anti-apoptotic proteins Bcl-XL and Myeloid cell leukaemia differentiation protein 1 (Mcl-1) were expressed
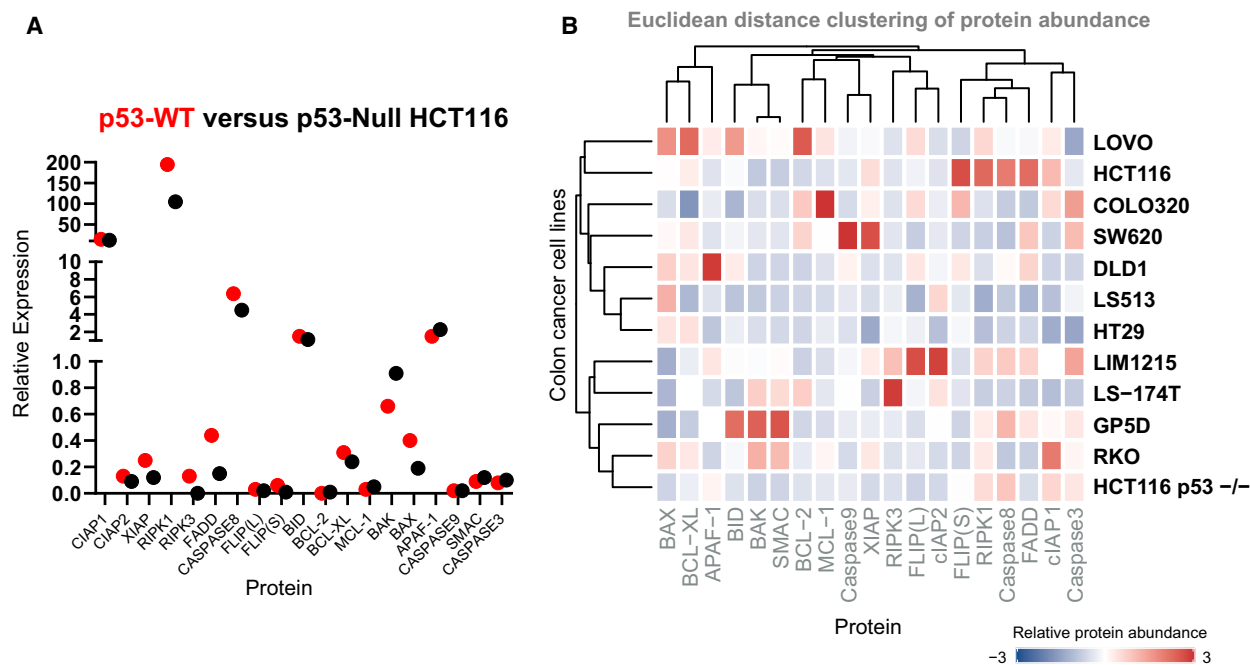
Fig. 3. Patterns of IAP interactome protein expression. (A) IAP interactome protein expression in isogenic HCT116 p53 WT and p53 null models. (B) Euclidean distance clustering of protein abundance. Relative protein abundance represented by z-score.

in all models albeit to varying degrees, whereas Bcl-2 itself was undetectable in half the models. While one of the requisite effectors for initiating MOMP, BCL2 antagonist/killer (BAK), was expressed in all models, BCL2-associated X-protein (BAX) was very low or absent in several models. A key component of the apoptosome, Apoptosis-associated factor-1 (APAF-1), was expressed variably across the panel, whilst procaspase-9, with which it forms the apoptosis-inducing apoptosome downstream of cytochrome c release from the mitochondria, was expressed in all models, albeit at a relatively low level compared with APAF-1, suggesting that procaspase-9 levels are likely the limiting factor for apoptosome formation. SMAC, like cytochrome c, is a key regulator of apoptosis downstream of MOMP that once released from mitochondria binds to and inhibits or promotes the degradation of IAPs [29]. Indeed, first-generation IAP antagonists such as Bir are based on the critical N-terminal domain of SMAC and are sometimes called SMAC mimetics [14,30]. SMAC was expressed in every model in the panel. Finally, the proform of the key executioner caspase, caspase-3, was expressed at a similar level in all models, suggestive of comparable potential to engage the executioner phase of apoptosis across the panel.

p53 is a key regulator of apoptosis signalling genes [31]. We therefore compared the expression of each protein in the isogenic p53 wild-type (WT) and Null

HCT116 models (Fig. 3A). Overall, the majority of proteins were constitutively expressed at a similar level in the presence and absence of p53. The canonical p53 target BAX was indeed higher in the p53 WT model. FADD and RIPK1 were also higher in the p53 WT setting, and consistent with our recent findings, FLIP was expressed more highly at the protein level in p53 WT HCT116 cells [32] as was XIAP. Moreover, hierarchical clustering did not reveal any differential patterns of protein expression between mutant and WT p53 models (Fig. 3B), suggesting that p53 status is not a major determinant of baseline apoptotic potential in CRC.

Correlation between IAP antagonist response and apoptotic protein expression

We next assessed whether the level of any of the individual proteins correlated with apoptosis induction. Linear correlation was determined using Pearson's correlation. In addition, Spearman's correlation was considered for the discovery of other monotonic dependencies and for the exclusion of outlier-driven linear correlation cases (Fig. 4). None of the IAP concentrations were correlated with Bir+TNF-α treatment; therefore, IAP levels alone were not separating responders to this combination. However, absolute levels of procaspase-8 positively correlated with response to

A

Pearson's correlation

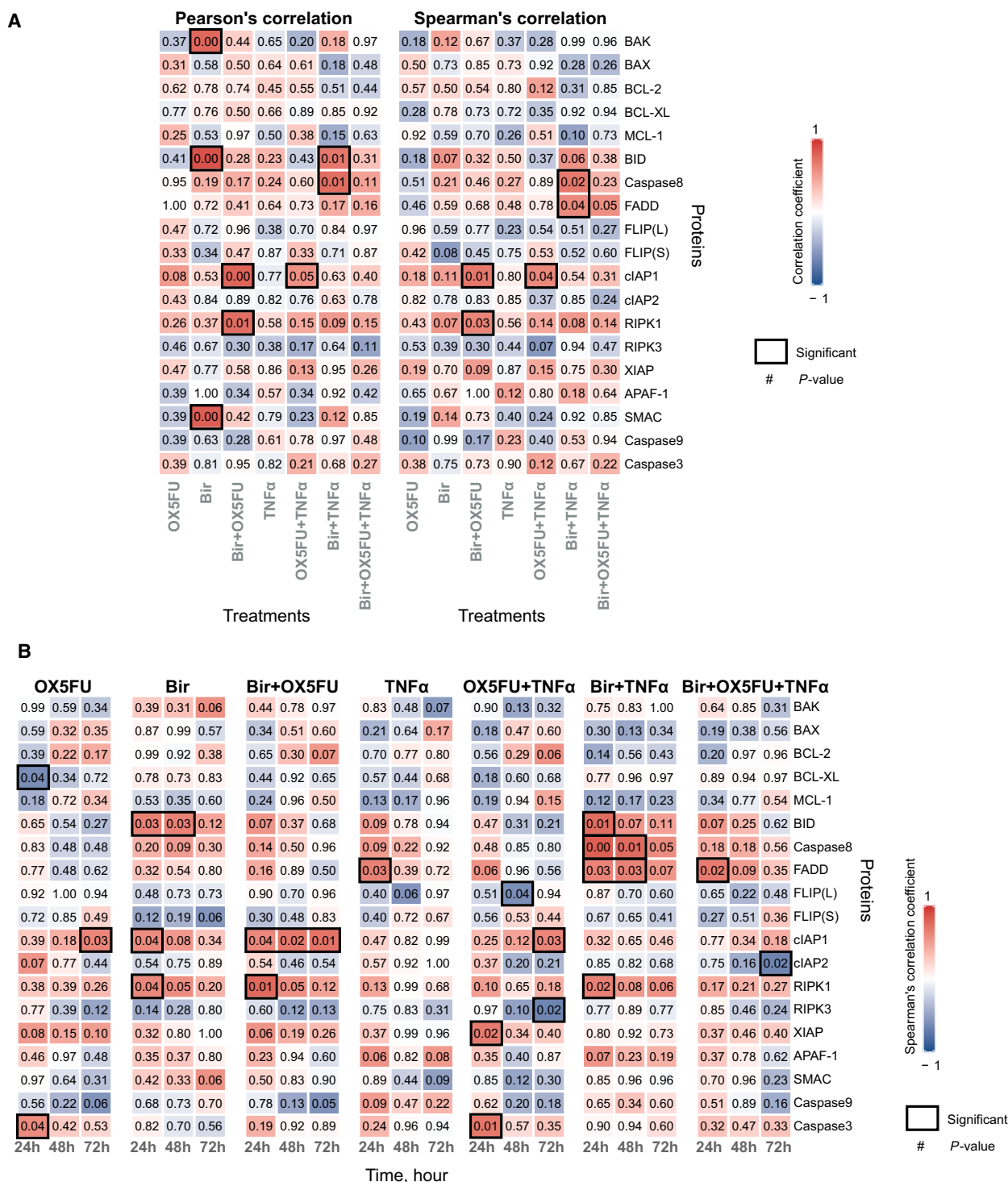| Protein	OX5FU	Bir	Bir+OX5FU	TNFα	OX5FU+TNFα	Bir+TNFα	Bir+OX5FU+TNFα
BAK	0.37	0.00	0.44	0.65	0.20	0.18	0.97
BAX	0.31	0.58	0.50	0.64	0.61	0.18	0.48
BCL-2	0.62	0.78	0.74	0.45	0.55	0.51	0.44
BCL-XL	0.77	0.76	0.50	0.66	0.89	0.85	0.92
MCL-1	0.25	0.53	0.97	0.50	0.38	0.15	0.63
BID	0.41	0.00	0.28	0.23	0.43	0.01	0.31
Caspase8	0.95	0.19	0.17	0.24	0.60	0.01	0.11
FADD	1.00	0.72	0.41	0.64	0.73	0.17	0.16
FLIP(L)	0.47	0.72	0.96	0.38	0.70	0.84	0.97
FLIP(S)	0.33	0.34	0.47	0.87	0.33	0.71	0.87
cIAP1	0.08	0.53	0.00	0.77	0.05	0.63	0.40
cIAP2	0.43	0.84	0.89	0.82	0.76	0.63	0.78
RIPK1	0.26	0.37	0.01	0.58	0.15	0.09	0.15
RIPK3	0.46	0.67	0.30	0.38	0.17	0.64	0.11
XIAP	0.47	0.77	0.58	0.86	0.13	0.95	0.26
APAF-1	0.39	1.00	0.34	0.57	0.34	0.92	0.42
SMAC	0.39	0.00	0.42	0.79	0.23	0.12	0.85
Caspase9	0.39	0.63	0.28	0.61	0.78	0.97	0.48
Caspase3	0.39	0.81	0.95	0.82	0.21	0.68	0.27

Spearman's correlation

Protein	OX5FU	Bir	Bir+OX5FU	TNFα	OX5FU+TNFα	Bir+TNFα	Bir+OX5FU+TNFα
BAK	0.18	0.12	0.67	0.37	0.28	0.99	0.96
BAX	0.50	0.73	0.85	0.73	0.92	0.28	0.26
BCL-2	0.57	0.50	0.54	0.80	0.12	0.31	0.85
BCL-XL	0.28	0.78	0.73	0.72	0.35	0.92	0.94
MCL-1	0.92	0.59	0.70	0.26	0.51	0.10	0.73
BID	0.18	0.07	0.32	0.50	0.37	0.06	0.38
Caspase8	0.51	0.21	0.46	0.27	0.89	0.02	0.23
FADD	0.46	0.59	0.68	0.48	0.78	0.04	0.05
FLIP(L)	0.96	0.59	0.77	0.23	0.54	0.51	0.27
FLIP(S)	0.42	0.08	0.45	0.75	0.53	0.52	0.60
cIAP1	0.18	0.11	0.01	0.80	0.04	0.54	0.31
cIAP2	0.82	0.78	0.83	0.85	0.37	0.85	0.24
RIPK1	0.43	0.07	0.03	0.56	0.14	0.08	0.14
RIPK3	0.53	0.39	0.30	0.44	0.07	0.94	0.47
XIAP	0.19	0.70	0.09	0.87	0.15	0.75	0.30
APAF-1	0.65	0.67	1.00	0.12	0.80	0.18	0.64
SMAC	0.19	0.14	0.73	0.40	0.24	0.92	0.85
Caspase9	0.10	0.99	0.17	0.23	0.40	0.53	0.94
Caspase3	0.38	0.75	0.73	0.90	0.12	0.67	0.22

Proteins

Treatments · Treatments

Correlation coefficient — 1 to −1

Significant · # P-value

B

Protein	OX5FU 24h	48h	72h	Bir 24h	48h	72h	Bir+OX5FU 24h	48h	72h	TNFα 24h	48h	72h	OX5FU+TNFα 24h	48h	72h	Bir+TNFα 24h	48h	72h	Bir+OX5FU+TNFα 24h	48h	72h
BAK	0.99	0.59	0.34	0.39	0.31	0.06	0.44	0.78	0.97	0.83	0.48	0.07	0.90	0.13	0.32	0.75	0.83	1.00	0.64	0.85	0.31
BAX	0.59	0.32	0.35	0.87	0.99	0.57	0.34	0.51	0.60	0.21	0.64	0.17	0.18	0.47	0.60	0.30	0.13	0.34	0.19	0.38	0.56
BCL-2	0.39	0.22	0.17	0.99	0.92	0.38	0.65	0.30	0.07	0.70	0.77	0.80	0.56	0.29	0.06	0.14	0.56	0.43	0.20	0.97	0.96
BCL-XL	0.04	0.34	0.72	0.78	0.73	0.83	0.44	0.92	0.65	0.57	0.44	0.68	0.18	0.60	0.68	0.77	0.96	0.97	0.89	0.94	0.97
MCL-1	0.18	0.72	0.34	0.53	0.35	0.60	0.24	0.96	0.50	0.13	0.17	0.96	0.19	0.94	0.15	0.12	0.17	0.23	0.34	0.77	0.54
BID	0.65	0.54	0.27	0.03	0.03	0.12	0.07	0.37	0.68	0.09	0.78	0.94	0.47	0.31	0.21	0.01	0.07	0.11	0.07	0.25	0.62
Caspase8	0.83	0.48	0.48	0.20	0.09	0.30	0.14	0.50	0.96	0.09	0.22	0.92	0.48	0.85	0.80	0.00	0.01	0.05	0.18	0.18	0.56
FADD	0.77	0.48	0.62	0.32	0.54	0.80	0.16	0.89	0.50	0.03	0.39	0.72	0.06	0.96	0.56	0.03	0.03	0.07	0.02	0.09	0.35
FLIP(L)	0.92	1.00	0.94	0.48	0.73	0.73	0.90	0.70	0.96	0.40	0.06	0.97	0.51	0.04	0.94	0.87	0.70	0.60	0.65	0.22	0.48
FLIP(S)	0.72	0.85	0.49	0.12	0.19	0.06	0.30	0.48	0.83	0.40	0.72	0.67	0.56	0.53	0.44	0.67	0.65	0.41	0.27	0.51	0.36
cIAP1	0.39	0.18	0.03	0.04	0.08	0.34	0.04	0.02	0.01	0.47	0.82	0.99	0.25	0.12	0.03	0.32	0.65	0.46	0.77	0.34	0.18
cIAP2	0.07	0.77	0.44	0.54	0.75	0.89	0.54	0.46	0.64	0.57	0.92	1.00	0.37	0.20	0.21	0.85	0.82	0.68	0.75	0.16	0.02
RIPK1	0.38	0.39	0.26	0.04	0.05	0.20	0.01	0.05	0.12	0.13	0.99	0.68	0.10	0.65	0.18	0.02	0.08	0.06	0.17	0.21	0.27
RIPK3	0.77	0.39	0.12	0.14	0.28	0.80	0.60	0.12	0.13	0.75	0.83	0.31	0.97	0.10	0.02	0.77	0.89	0.77	0.85	0.46	0.24
XIAP	0.08	0.15	0.10	0.32	0.80	1.00	0.06	0.19	0.26	0.37	0.99	0.96	0.02	0.34	0.40	0.80	0.92	0.73	0.37	0.46	0.40
APAF-1	0.46	0.97	0.48	0.35	0.37	0.80	0.23	0.94	0.60	0.06	0.82	0.08	0.35	0.40	0.87	0.07	0.23	0.19	0.37	0.78	0.62
SMAC	0.97	0.64	0.31	0.42	0.33	0.06	0.50	0.83	0.90	0.89	0.44	0.09	0.85	0.12	0.30	0.85	0.96	0.96	0.70	0.96	0.23
Caspase9	0.56	0.22	0.06	0.68	0.73	0.70	0.78	0.13	0.05	0.09	0.47	0.42	0.62	0.20	0.18	0.65	0.34	0.60	0.51	0.89	0.16
Caspase3	0.04	0.42	0.53	0.82	0.70	0.56	0.19	0.92	0.89	0.24	0.96	0.94	0.01	0.57	0.35	0.90	0.94	0.60	0.32	0.47	0.33

Proteins

Time, hour

Spearman's correlation coefficient — 1 to −1

Significant · # P-value

Fig. 4. Correlation between proteins and specific cell death for individual treatments. (A) Heat map shows Pearson's and Spearman's correlation coefficients (colour bar) between the concentration of 19 proteins and specific cell death in 12 colon cancer cell lines for TNF-α, OX5FU and Bir combinational treatments. Specific cell death was averaged over three time points. Numbers indicate P-values. The significant correlations are highlighted in black frames. (B) Heat map shows Spearman's correlation coefficients (colour bar) between the concentration of 19 proteins and specific cell death at 24, 48 and 72 h for all treatments. Numbers indicate P-values.
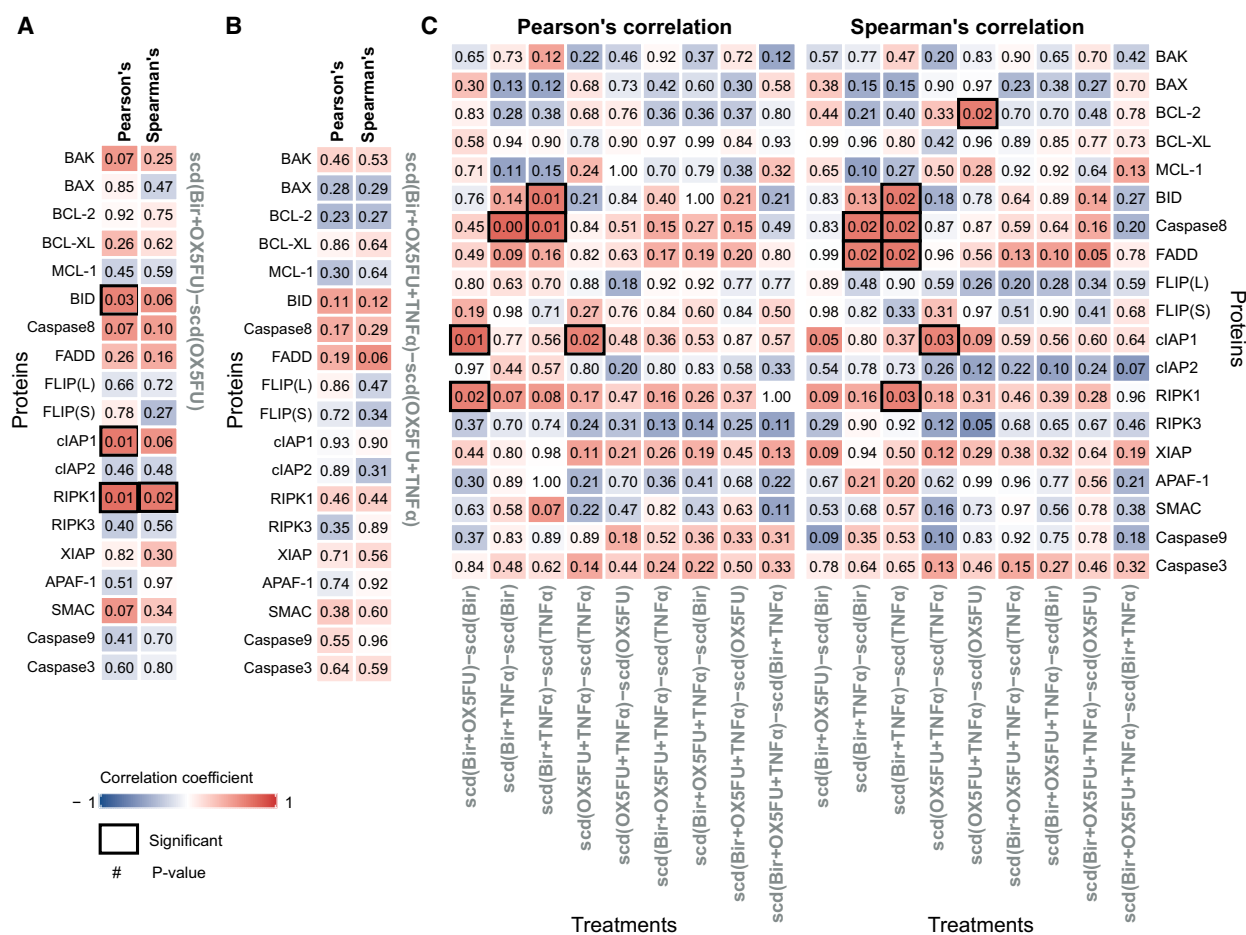
Fig. 5. Correlation between individual proteins and specific cell death (scd) difference. (A) Correlation between individual proteins and averaged specific cell death (scd) difference between Bir+OX5FU and OX5FU treatments. (B) Correlation between individual proteins and averaged specific cell death (scd) difference between Bir+OX5FU+TNF-α and OX5FU+TNF-α treatments. (C) Heat map shows Pearson's and Spearman's correlation coefficients (colour bar) between the concentration of 19 proteins and difference in response between the following treatments: Bir+OX5FU and Bir; Bir+TNF-α and Bir; Bir+TNF-α and TNF-α; OX5FU+TNF-α and TNF-α; OX5FU+TNF-α and OX5FU; Bir+OX5FU+TNF-α and TNF-α; Bir+OX5FU+TNF-α and Bir; Bir+OX5FU+TNF-α and OX5FU; Bir+OX5FU+TNF-α and Bir+TNF-α. Response difference was calculated from specific cell death averaged over three time points. Numbers indicate *P*-values.

Bir+TNF-α (Fig. 4A), and this effect was robust across all three time points (Fig. 4B). cIAP1 expression was found to be significantly correlated with response to Bir+OX5FU, as was response to OX5FU+TNF-α; this suggests that sensitivity to chemotherapy is related to cIAP1 expression, and indeed, there was a non-significant trend for cIAP1 expression and response to OX5FU (Pearson's $r = 0.52$, $P = 0.08$). Moreover, the increase in cell death between Bir+OX5FU and OX5FU treatments (Fig. 5A) or between Bir+OX5FU and Bir treatments (Fig. 5C) also showed a linear dependence on cIAP1 levels; however, this relationship was not found to be significant in Spearman's correlation test (Fig. 5A,C) and was lost following the addition of TNF-α (Fig. 5B).

Notably, RIPK1 was found to be a more prominent indicator of the Bir+OX5FU response. Its level was significantly correlated with Bir+OX5FU response using both Pearson's and Spearman's tests (Fig. 4A), especially after 24 h (Fig. 4B). In addition, RIPK1 was also found to be correlated with the increase in cell death response between Bir+OX5FU and OX5FU treatments (Fig. 5A).

Minimal apoptotic protein profile that separates treatment responses by means of linear discriminant models

From our protein quantification experiments, 19 proteins that characterise the extrinsic and intrinsic
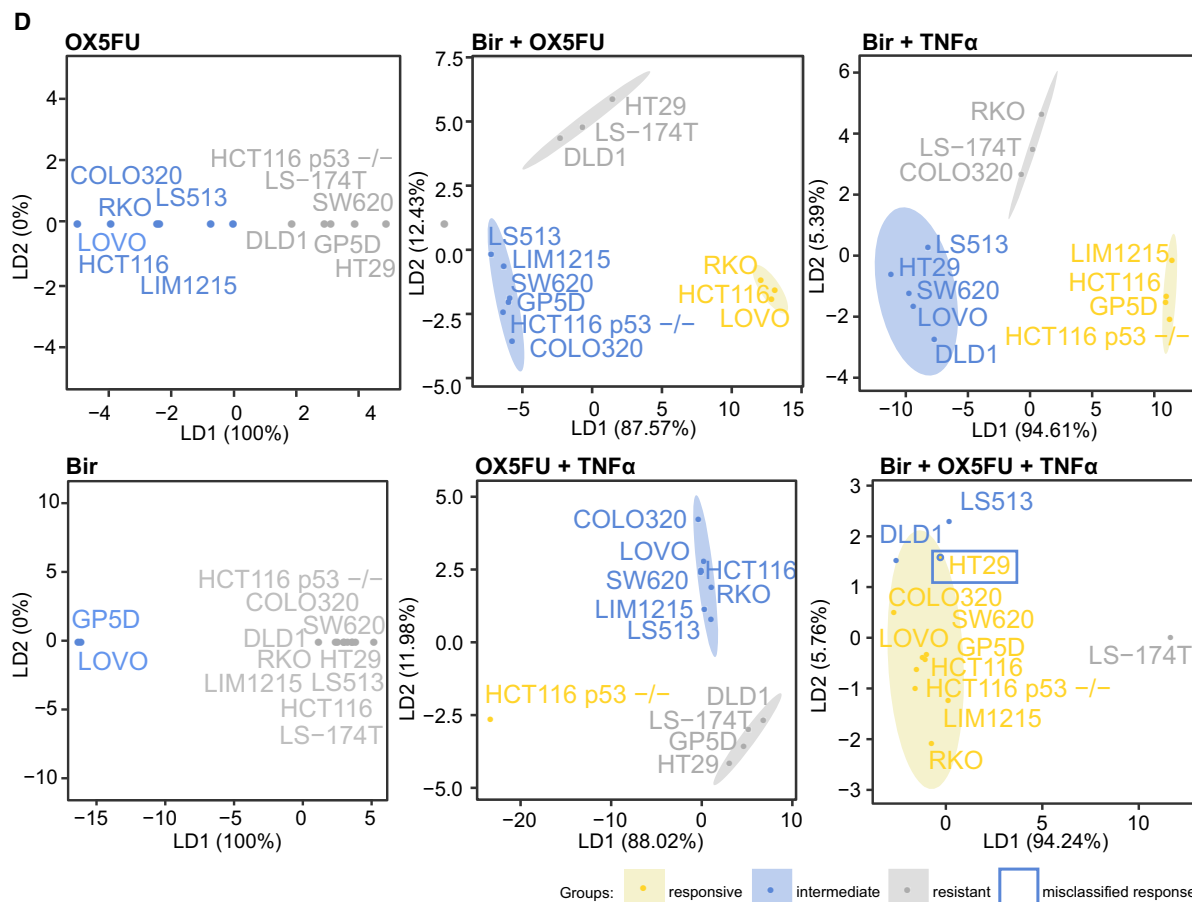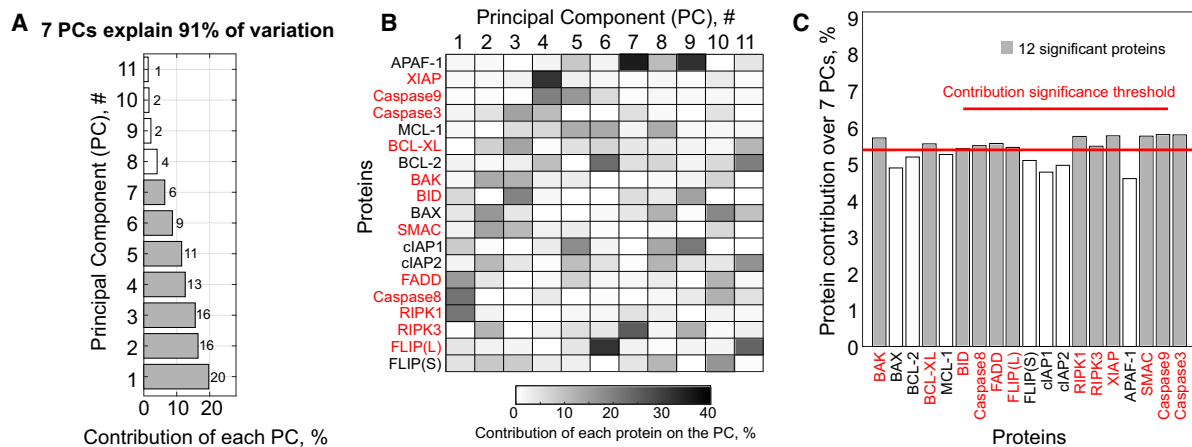
apoptotic pathways showed a wide range of variance and amplitude over the 12 cell lines (Fig. 2B, Table 2). To identify proteins and minimal characteristic protein profiles that separated responses, we performed a principal component analysis (PCA) (Fig. 6A-C). PCA discovered 11 component axes (principal components, PCs) that transformed the 19 proteins set into a system of coordinates that optimally captured the protein expression variance of our cell line profiles (Fig. 6A). Based on PC eigenvalues, we have found that first seven PCs cumulatively captured 91% of the variation we measured in the protein profiles. Thus, these seven PCs were kept as essential components for the subsequent analysis. Interestingly, we noted that the first PC which explained 20% of the entire variance in the protein profiles showed a very strong dependence on the core components of the Ripoptosome complex: FADD, caspase-8 and RIPK1 (Fig. 6B). It is known that downstream of IAP inhibitor treatment, the cytosolic Ripoptosome is the signalling platform required for the activation of initiator caspase, procaspase-8, thus triggering the extrinsic apoptosis pathway response [33–35]. Moreover, Ripoptosome assembly on its own contributes to a high variability in the cell death response as shown in experimental and mathematical modelling studies [36,37]. Thus, our results suggested that the capacity to initiate extrinsic apoptosis through the Ripoptosome might be a prominent process that is affected by protein expression differences between our cell lines. To identify a minimal protein set, the contribution of each protein was averaged over the first seven essential PCs (Fig. 6C). From this, we could down select 12 proteins that are involved in the extrinsic (FADD, caspase-8, RIPK1, RIPK3, FLIP(S), BID) and in the intrinsic (XIAP, caspase-9, caspase-3, BCL-XL, BAK, SMAC) apoptosis pathways.

To find the relationship between these proteins and cell death responses, we categorised cell lines into 3 response groups according to treatment-specific cell death averaged over 3 time points (Table 3). Groups 'resistant', 'intermediate' and 'responsive' were assigned for cell death response < 10%, 10–30% and > 30%, respectively. Thus, the specific cell death

responses were discretised for further comparison with the minimal protein set by means of linear discriminant analysis (LDA) [38–41]. LDA provides a linear classification model that transforms the minimal protein set into a new subspace of component axes that maximises the separation of the response groups. These axes are called linear discriminant functions (LDs) and were generated for each treatment separately (Fig. 6D). An important property of LDA is that its performance is independent of the protein data standardisation because the algorithm relies on variation between response groups only. Therefore, LDs are the linear functions of protein concentrations directly and, therefore, can be used for response classification in any data set expressed in concentration terms. The scatter plots showed clear separation between all response groups in the optimal LD spaces calculated for OX5FU, Bir+OX5FU and Bir+TNF-α treatments (Fig. 6D) with 100% accuracy in response classification for all 12 cell lines (Fig. 6E).

Descriptive accuracy of the LDA models was achieved for most of our treatments with the minimal set of 12 proteins. Only one classification error occurred for the Bir+OX5FU+TNF-α treatment in the classification of HT29 cells. In this case, the LDA model underestimated the HT29 response, suggesting for it an intermediate rather than a responsive group (Fig. 6D, E). This inaccuracy was found to be associated with the overall weaker separation between response groups for the triple-treatment combination LDA model. This was likely due to the underrepresentation of intermediate and resistant response groups (2 and 1 cell lines are representing these two groups, respectively) or an influence of other key signalling pathways not covered in the present study. Nevertheless, cell lines that are resistant to Bir+OX5FU and, at the same time, responsive to Bir+TNF-α all show a high level of response to Bir+OX5FU+TNF-α. Additionally, all cell lines responsive to Bir+OX5FU were also responsive to Bir+OX5FU+TNF-α. Therefore, the Bir+OX5FU+TNF-α LDA model (Fig. 6D), which did not separate well, is dispensable, and the triple-treatment responsive cell lines can be identified from the use of the Bir+OX5FU and Bir+TNF-α LDA models.

Fig. 6. Protein profile minimisation through PCA and treatment-wise LDA of minimised protein profiles. (A) Contribution of each PC into the variance among apoptotic protein profiles in 12 colon cancer cell lines. First seven PCs explain 91% of the variation. (B) Contribution of each individual protein on each individual PC. (C) Combined contribution of the first seven PCs redistributed over 19 individual proteins. Twelve proteins have shown significant contribution (grey bars) and considered as the minimal protein profile. (D) LD functions of the minimal protein profiles that separate treatment response groups for OX5FU, Bir+OX5FU, Bir+TNF-α, Bir, OX5FU+TNF-α and Bir+OX5FU+TNF-α. LDA for each separate treatment was based on the response groups that were derived from treatment-specific cell death averaged over three time points. (E) Accuracy of LDA models for all treatments.

A **7 PCs explain 91% of variation**

B

C

D

Groups: ● responsive   ● intermediate   ● resistant   □ misclassified response

E

Accuracy of the LDA models

Treatment	Correctly grouped colon cancer cell lines, %
Bir	100%
OX5FU	100%
Bir + OX5FU	100%
Bir + TNFα	100%
OX5FU + TNFα	100%
Bir + OX5FU + TNFα	91%

HT29 was misclassified by LDA model for Bir+OX5FU+TNFα treatment:
Predicted by LDA: intermediate (10–30%)
Actual: responsive (54.21%)

Table 3. Specific cell death classification. 12 colon cancer cell lines have been categorised into three response groups according to the treatment-specific cell death averaged over three time points (24, 48 and 72 h). Groups resistant (grey), intermediate (blue) and responsive (yellow) were assigned for cell death response < 10%, 10–30% and > 30%, respectively.

Model	Treatments						
	Bir	OX 5FU	Bir OX5FU	Bir TNF-α	OX5FU TNF-α	Bir OX5FU TNF-α	TNF-α
DLD1	0.62	1.63	1.84	11.22	2.71	17.52	2.37
LS174T	2.54	2.68	7.01	9.42	4.92	4.65	1.06
LOVO	12.03	16.58	38.96	28.38	22.41	38.02	7.14
HT29	0.20	2.18	5.76	17.25	3.84	54.21	-0.53
GP5D	25.23	1.04	27.97	61.27	5.92	60.85	5.12
LIM1215	2.24	17.03	23.29	37.08	16.55	55.29	1.27
HCT116	3.18	19.07	46.10	31.35	28.55	56.89	3.51
RKO	4.60	17.48	43.05	9.91	20.95	37.95	-2.11
SW620	1.06	6.30	10.39	22.18	23.82	63.33	4.09
COLO320	-0.54	18.64	17.67	1.83	23.95	32.54	0.83
LS513	1.73	20.27	23.44	11.73	22.32	25.80	5.63
HCT116 p53$^{-/-}$	4.52	6.72	19.26	42.01	31.45	65.92	7.41

Clinical Positioning of IAP inhibitors in CRC

Overall, our analyses suggest that benefit from the treatment with IAP inhibitors in CRC can be calculated from the use of a panel of 12 proteins plus knowledge of whether the tumour is inflamed (indicating the presence of TNF-α). As depicted in Fig. 7, if the protein profile indicates that a tumour is in the 'Bir+OX5FU responsive' group, the patient would be predicted to benefit from treatment with an IAP inhibitor alongside FOLFOX. If not, consideration would be given to whether the patient's tumour expresses TNF-α. If inflammation is present and the patient's tumour falls into the 'Bir+TNF-α responsive' group, the patient would be predicted to benefit from treatment with an IAP inhibitor. If not, the benefits of the combinational treatment with an IAP antagonist would be predicted to be minimal.

To make the above approach clinically feasible, simple protein quantification approaches are needed. In this regard, huge advances in multiplex immunohistochemistry have been made. For example, a multiplexed fluorescence microscopy method for the quantification of multiple proteins from formalin-fixed paraffin-embedded tissues was recently described that can quantify up to 60 proteins in single 5-μm sections [42,43]. The ability to do this analysis in single sections means problems of changing cellularity associated with sequential sectioning needed for traditional IHC (one section per protein) are overcome. This and similar methodologies can also identify the presence of specific immune cell populations in tumours and hence whether or not a tissue is inflamed. Conversion of protein intensities into absolute concentrations would require the incorporation of

standards into the analysis; this could be achieved using formalin-fixed cell lines with known protein concentrations embedded alongside the tumour sample. Thus, these emerging approaches could be employed to convert experimentally derived proteomics-based predictive algorithms such as we have developed here into real-world companion diagnostics.

Materials and methods

CRC cell line panel

Cell lines were selected as a representation of the molecular genetic diversity seen in CRC based on the mutation status of known driver genes (including TP53, KRAS, BRAF and PIK3CA), transcriptional profiling and microsatellite stability status, as published in Medico et al. [15]. HeLa, DLD1, LS174T, LoVo, HT29, GP5D, LIM1215, HCT116, RKO, SW620, COLO320 and LS513 cell lines were purchased as authenticated stocks from ATCC (Teddington, UK). HCT116 p53$^{-/-}$ was gifted from B. Vogelstein (Johns Hopkins University, USA). Immediately after purchase, early passage stocks of each cell line were frozen down. After thawing, cells were kept for a limited number of passages and were regularly screened for the presence of mycoplasma using the MycoAlert Mycoplasma Detection Kit (Lonza, Basel, Switzerland).

Protein quantification, recombinant proteins and western blotting

Quantitative western blotting was carried out as previously described [16]. cIAP1, cIAP2 and caspase-8 antibodies were
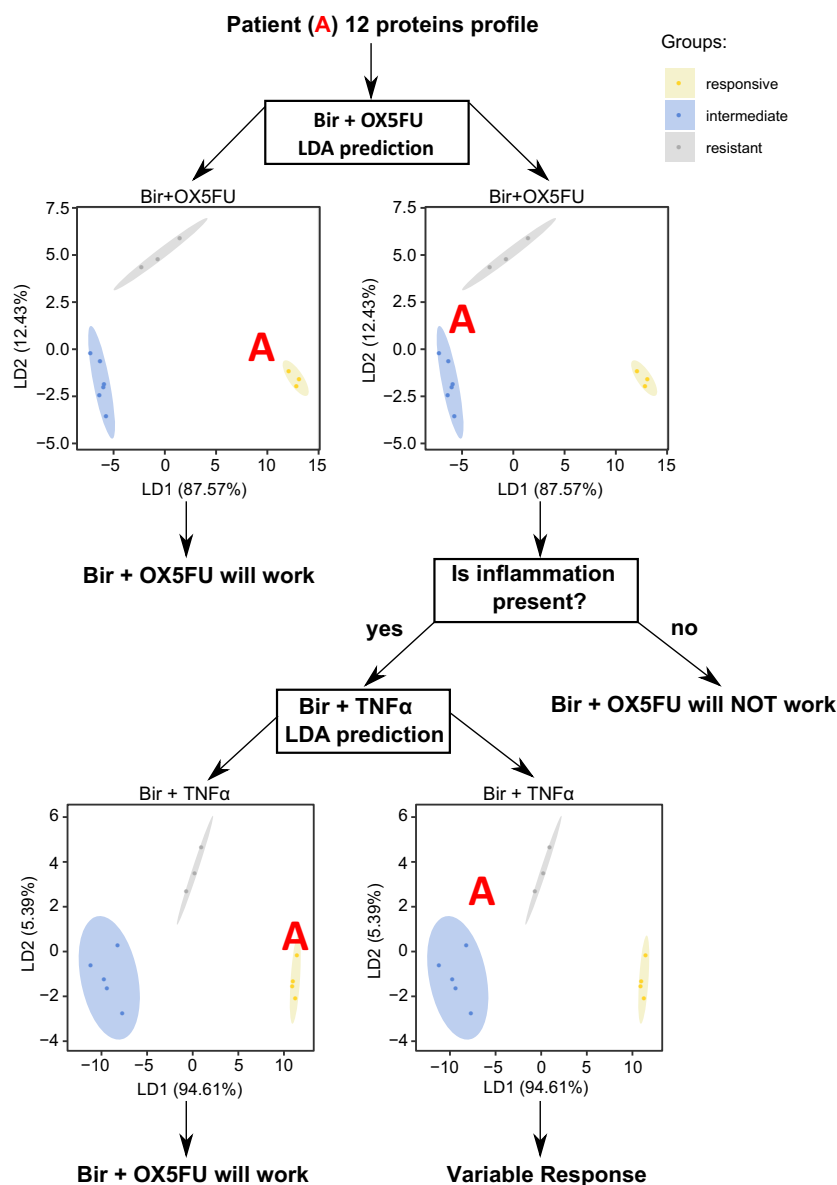
Fig. 7. Prediction pipeline. LDA-based algorithm for clinical prediction of benefit from treatment with an IAP inhibitor alongside SoC chemotherapy.

obtained from Enzo (Exeter, UK). FLIP antibody was purchased from AdipoGen (San Diego, CA, USA). RIPK1, RIPK3, XIAP, caspase-3, caspase-9, SMAC, Bid, BCL-2, BCL-XL, MCL-1, Bax, Bak APAF-1 and cytochrome c antibodies were purchased from Cell Signaling Technology (Danvers, MA, USA). β-actin antibody was purchased from Sigma (St. Louis, MO, USA). Fluorophore-labelled secondary antibodies were acquired from LI-COR Biosciences (Lincoln, NE, USA). Images were captured using an Odyssey Imaging System (LI-COR) at 12-bit dynamic range. Protein expression in reference cell lines (HeLa/HT29) was quantified against a standard curve of recombinant protein standards or previously quantified and was used to determine absolute quantities in the cell line panel. Recombinant RIPK1, RIPK3, cIAP1, cIAP2 and XIAP

were purchased from Abnova (Taoyuan, Taiwan). p-18 caspase-8 was acquired from Sigma, and FLIP and FADD were produced in-house (PGJCCR, Queen's University Belfast) as described in Majkut *et al.* [17]. Recombinant Bid, BCL-2, BCL-XL, MCL-1, Bax, Bak, APAF-1, procaspase-9, procaspase-3 and SMAC were used to quantify absolute protein concentrations as previously published [16,18].

Cell death assay

Sensitivity of CRC cell lines to each treatment was determined by Annexin V/propidium iodide high-content microscopy. Cells were seeded at appropriate densities and treated for 24, 48 or 72 h with TL32711 (Bir; Selleck Chemicals, Munich, Germany) alone, chemotherapy alone ['OX5FU':

10 μM 5FU (Medac, Chobham, Surrey, UK) plus 2 μM oxaliplatin (Accord, Barnstaple, Devon, UK)], or a combination of the two in the presence or absence of 10 ng·mL^{-1} TNF-α (Alomone Labs, Jerusalem, Israel). Cells were stained with propidium iodide (Sigma, UK), FITC-labelled Annexin V (Thermo Fisher, Waltham, MA, USA) and Hoechst 33342 to visualise nuclei (Thermo Fisher). Cell death was quantified (AV+and/or PI+) on an Array Scan XTI high-content microscope (Thermo Scientific). To control for variabilities in basal cell death across the CRC panel, treatment-specific cell death was calculated as follows: {cell death in treatment group} – {cell death in control group}.

Statistics

Pairwise comparisons of the mean treatment responses with the Wilcoxon test were performed using ggpubr v0.3.0 package [19] together with the ggplot2 v3.3.0 package [20] in the R environment [21]. Spearman's and Pearson's correlation coefficients were calculated to identify significant correlations between cell line sensitivities (treatment-specific cell death) and absolute concentrations of each IAP interactome protein. Correlation and hierarchical clustering heat maps were produced with the R package clusterProfiler v3.12.0 [22]. PCA was applied for dimensionality reduction in the characteristic protein profile in the cohort of 12 colon cancer cell lines (Fig. 6A). For the PCA, we standardised protein concentrations (z-scores of 19 proteins). We have calculated the contribution of each protein on the given PC (Fig. 6B) from the correlation coefficients between a protein and PC termed loadings of variables as per the following: $\text{Contribution}(i,j) = \frac{(\text{loading}(i,j))^2 \times 100\%}{\sum_{j=1}^{19}(\text{loading}(i,j))^2}$, where $1 \leq i \leq 11$ is the indexing of PCs, and $1 \leq j \leq 19$ is the indexing of proteins [23].

Further, the contribution of each protein over first seven PCs (Fig. 6C) was calculated as follows: $\text{Contr}(j) = \frac{\sum_{i=1}^{7}(\text{Contribution}(i,j) \times \lambda(i))}{\sum_{i=1}^{7} \lambda(i)}$, where $\lambda(i)$ is the eigenvalue of PC$_i$. With the assumption of average uniform expected contribution for all 19 proteins, the significance threshold was set to 5.26%. PCA algorithm was implemented using MATLAB 2017b [24]. LDA was then performed on the minimised protein profile (12 proteins), using absolute protein concentrations, and categorical response groups assigned based on specific cell death averaged over three time points (24, 48 and 72 h). LDA runs were performed for each treatment independently with R package MASS v7.3-51.5 [25].

Conflict of interest

DBL has received funding support from Astex Pharmaceuticals and acted as an advisor on the development of their IAP inhibitor tolinapant.

Author contributions

CMcC acquired, analysed and interpreted the data, and drafted the manuscript. AM analysed and interpreted the data, and drafted the manuscript. KM analysed and interpreted the data and drafted the manuscript. SVS supervised the project. TS analysed the data. MF acquired the data and analysed the manuscript. SC acquired and analysed the data. MR acquired funding, interpreted the data and drafted the manuscript. JHMP acquired funding, supervised the project, interpreted the data and drafted the manuscript. DBL acquired funding, supervised the project, interpreted the data and drafted the manuscript.

Peer Review

The peer review history for this article is available at https://publons.com/publon/10.1111/febs.15801.

References

1 Holohan C, Van Schaeybroeck S, Longley DB & Johnston PG (2013) Cancer drug resistance: an evolving paradigm. *Nat Rev Cancer* **13**, 714–726.

2 Hector S & Prehn JHM (2009) Apoptosis signaling proteins as prognostic biomarkers in colorectal cancer: a review. *Biochim Biophys Acta* **1795**, 117–129.

3 Darding M & Meier P (2012) IAPs: guardians of RIPK1. *Cell Death Differ* **19**, 58–66.

4 Vanden Berghe T, Linkermann A, Jouan-Lanhouet S, Walczak H & Vandenabeele P (2014) Regulated necrosis: the expanding network of non-apoptotic cell death pathways. *Nat Rev Mol Cell Biol* **15**, 135–147.

5 Dondelinger Y, Darding M, Bertrand MJM & Walczak H (2016) Poly-ubiquitination in TNFR1-mediated necroptosis. *Cell Mol Life Sci* **73**, 2165–2176.

6 Deveraux QL, Takahashi R, Salvesen GS & Reed JC (1997) X-linked IAP is a direct inhibitor of cell-death proteases. *Nature* **388**, 300–304.

7 Eckelman BP & Salvesen GS (2006) The human anti-apoptotic proteins cIAP1 and cIAP2 bind but do not inhibit caspases. *J Biol Chem* **281**, 3254–3260.

8 Feltham R, Bettjeman B, Budhidarmo R, Mace PD, Shirley S, Condon SM, Chunduru SK, McKinlay MA, Vaux DL, Silke J *et al.* (2011) Smac mimetics activate the E3 ligase activity of cIAP1 protein by promoting RING domain dimerization. *J Biol Chem* **286**, 17015–17028.

9 Crawford N, Stasik I, Holohan C, Majkut J, McGrath M, Johnston PG, Chessari G, Ward GA, Waugh DJ, Fennell DA *et al.* (2013) SAHA overcomes FLIP-mediated inhibition of SMAC mimetic-induced apoptosis in mesothelioma. *Cell Death Dis* **4**, e733.

10 McCann C, Crawford N, Majkut J, Holohan C, Armstrong CWD, Maxwell PJ, Ong CW, LaBonte MJ, McDade SS, Waugh DJ *et al.* (2018) Cytoplasmic FLIP (S) and nuclear FLIP(L) mediate resistance of castrate-resistant prostate cancer to apoptosis induced by IAP antagonists. *Cell Death Dis* **9**, 1081.

11 Oberst A, Dillon CP, Weinlich R, McCormick LL, Fitzgerald P, Pop C, Hakem R, Salvesen GS & Green DR (2011) Catalytic activity of the caspase-8-FLIP(L) complex inhibits RIPK3-dependent necrosis. *Nature* **471**, 363–367.

12 Feoktistova M & Leverkus M (2015) Programmed necrosis and necroptosis signalling. *FEBS J* **282**, 19–31.

13 Ndubaku C, Varfolomeev E, Wang L, Zobel K, Lau K, Elliott LO, Maurer B, Fedorova AV, Dynek JN, Koehler M *et al.* (2009) Antagonism of c-IAP and XIAP proteins is required for efficient induction of cell death by small-molecule IAP antagonists. *ACS Chem Biol* **4**, 557–566.

14 Fulda S & Vucic D (2012) Targeting IAP proteins for therapeutic intervention in cancer. *Nat Rev Drug Discov* **11**, 109–124.

15 Medico E, Russo M, Picco G, Cancelliere C, Valtorta E, Corti G, Buscarino M, Isella C, Lamba S, Martinoglio B *et al.* (2015) The molecular landscape of colorectal cancer cell lines unveils clinically actionable kinase targets. *Nat Commun* **6**, 7002.

16 Lindner AU, Concannon CG, Boukes GJ, Cannon MD, Llambi F, Ryan D, Boland K, Kehoe J, McNamara DA, Murray F *et al.* (2013) Systems analysis of BCL2 protein family interactions establishes a model to predict responses to chemotherapy. *Cancer Res* **73**, 519–528.

17 Majkut J, Sgobba M, Holohan C, Crawford N, Logan AE, Kerr E, Higgins CA, Redmond KL, Riley JS, Stasik I *et al.* (2014) Differential affinity of FLIP and procaspase 8 for FADD's DED binding surfaces regulates DISC assembly. *Nat Commun* **5**, 3350.

18 Rehm M, Huber HJ, Dussmann H & Prehn JHM (2006) Systems analysis of effector caspase activation and its control by X-linked inhibitor of apoptosis protein. *EMBO J* **25**, 4338–4349.

19 Kassambara A (2020) ggpubr: "ggplot2" Based Publication Ready Plots.

20 Wickham H (2016) ggplot2: Elegant Graphics for Data Analysis Springer-Verlag, New York, NY.

21 R Core Team (2013) R: A Language and Environment for Statistical Computing. R Foundation for Statistical Computing, Vienna, Austria.

22 Yu G, Wang L-G, Han Y & He Q-Y (2012) clusterProfiler: an R package for comparing biological themes among gene clusters. *OMICS* **16**, 284–287.

23 Abdi H & Williams LJ (2010) Principal component analysis. *WIREs Comput Stat* **2**, 433–459.

24 MATLAB (2017) 9.3.0.713579 (R2017b). The MathWorks Inc., Natick, MA.

25 Venables WN & Ripley BD (2002) Modern Applied Statistics with S. Fourth Springer, New York, NY.

26 Humphreys LM, Fox JP, Higgins CA, Majkut J, Sessler T, McLaughlin K, McCann C, Roberts JZ, Crawford NT, McDade SS *et al.* (2020) A revised model of TRAIL-R2 DISC assembly explains how FLIP(L) can inhibit or promote apoptosis. *EMBO Rep* **21**, e49254.

27 Cory S & Adams JM (2002) The Bcl2 family: regulators of the cellular life-or-death switch. *Nat Rev Cancer* **2**, 647–656.

28 Luo X, Budihardjo I, Zou H, Slaughter C & Wang X (1998) Bid, a Bcl2 interacting protein, mediates cytochrome c release from mitochondria in response to activation of cell surface death receptors. *Cell* **94**, 481–490.

29 Adrain C, Creagh EM & Martin SJ (2001) Apoptosis-associated release of Smac/DIABLO from mitochondria requires active caspases and is blocked by Bcl-2. *EMBO J* **20**, 6627–6636.

30 Wu H, Tschopp J & Lin S-C (2007) Smac mimetics and TNFalpha: a dangerous liaison? *Cell* **131**, 655–658.

31 Fridman JS & Lowe SW (2003) Control of apoptosis by p53. *Oncogene* **22**, 9030–9040.

32 Lees A, McIntyre AJ, Crawford NT, Falcone F, McCann C, Holohan C, Quinn GP, Roberts JZ, Sessler T, Gallagher PF *et al.* (2020) The pseudo-caspase FLIP (L) regulates cell fate following pactivation. *Proc Natl Acad Sci USA* **117**, 17808–17819.

33 Bertrand MJM & Vandenabeele P (2011) The ripoptosome: death decision in the cytosol. *Mol Cell* **43**, 323–325.

34 Feoktistova M, Geserick P, Kellert B, Dimitrova DP, Langlais C, Hupe M, Cain K, MacFarlane M, Häcker G & Leverkus M (2011) cIAPs block Ripoptosome formation, a RIP1/caspase-8 containing intracellular cell death complex differentially regulated by cFLIP isoforms. *Mol Cell* **43**, 449–463.

35 Tenev T, Bianchi K, Darding M, Broemer M, Langlais C, Wallberg F, Zachariou A, Lopez J, MacFarlane M, Cain K *et al.* (2011) The Ripoptosome, a signaling

platform that assembles in response to genotoxic stress and loss of IAPs. *Mol Cell* **43**, 432–448.

36 Roux J, Hafner M, Bandara S, Sims JJ, Hudson H, Chai D & Sorger PK (2015) Fractional killing arises from cell-to-cell variability in overcoming a caspase activity threshold. *Mol Syst Biol* **11**, 803.

37 Matveeva A, Fichtner M, McAllister K, McCann C, Sturrock M, Longley DB & Prehn JHM (2019) Heterogeneous responses to low level death receptor activation are explained by random molecular assembly of the Caspase-8 activation platform. *PLoS Comput Biol* **15**, e1007374.

38 Fisher RA (1936) The use of multiple measurements in taxonomic problems. *Ann Eugen* **7**, 179–188.

39 Rao CR (1948) The utilization of multiple measurements in problems of biological classification†. *J R Stat Soc Ser B* **10**, 159–193.

40 Johnson AR & Wichern DW (1988) Applied multivariate statistical analysis. *Biometrics* **44**, 920.

41 Fukunaga K (1990) Chapter 1 - Introduction. In Introduction to Statistical Pattern Recognition, 2nd edn. (Fukunaga K, ed), pp. 1–10. Academic Press, Boston, MA.

42 Gerdes MJ, Sevinsky CJ, Sood A, Adak S, Bello MO, Bordwell A, Can A, Corwin A, Dinn S, Filkins RJ *et al.* (2013) Highly multiplexed single-cell analysis of formalin-fixed, paraffin-embedded cancer tissue. *Proc Natl Acad Sci USA* **110**, 11982–11987.

43 Schubert W, Bonnekoh B, Pommer AJ, Philipsen L, Böckelmann R, Malykh Y, Gollnick H, Friedenberger M, Bode M & Dress AWM (2006) Analyzing proteome topology and function by automated multidimensional fluorescence microscopy. *Nat Biotechnol* **24**, 1270–1278.